IOP Conf. Series: Materials Science and Engineering **192** (2017) 012009 doi:10.1088/1757-899X/192/1/012009

The evolution of structural and chemical heterogeneity during rapid solidification at gas atomization

V M Golod[1] and V Sh Sufiiarov[1]

[1] Peter the Great St.-Petersburg Polytechnic University, Institute of Metallurgy, Mechanical Engineering and Transport, Saint- Petersburg, 195251, Russia

e-mail: lpi2015@mail.ru

Abstract. Gas atomization is a high-performance process for manufacturing superfine metal powders. Formation of the powder particles takes place primarily through the fragmentation of alloy melt flow with high-pressure inert gas, which leads to the formation of non-uniform sized micron-scale particles and subsequent their rapid solidification due to heat exchange with gas environment. The article presents results of computer modeling of crystallization process, simulation and experimental studies of the cellular-dendrite structure formation and microsegregation in different size particles. It presents results of adaptation of the approach for local nonequilibrium solidification to conditions of crystallization at gas atomization, detected border values of the particle size at which it is possible a manifestation of diffusionless crystallization.

1. Introduction

A number of promising technological processes for manufacturing of the metal products are targeting to use micro-scale metallurgical blanks as raw materials, which are in contrast to the traditional large-scale ingots and castings having sizes $\approx 10^{-6}$ m. These primarily include selective laser melting, electron beam melting, direct metal deposition, cladding, spray forming, spark plasma sintering, extrusion, powder injection molding etc. Raw material for these processes usually produced by spinning processes, atomization (plasma, gas, water atomization), spray-based technologies et al [1-4]. Their appearance was due to a desire to get away from "birth defects" of the traditional technologies like coarse columnar structures in steel billets and castings, as well as macro- and micro segregation in combination with gaseous and nonmetallic inclusions. A transition to use micropowders provides a reduction in size microstructural parameters due to a sharp increase in crystallization rate and deep melts supercooling. A condition of local equilibrium at the liquid-solid phase interface is disrupted during rapid solidification as a result of increasing concentration and "trapping" of alloying components of the alloy, which leads to a sequent structural transition from dendrite to cellular and flat morphology with the establishment at the interface local nonequilibrium conditions, that in the limit gives diffusionless crystallization mode [3].

Atomization of the melt obtained through the fragmentation of alloy melt flow leads to an inhomogeneous array of small particles entrained by gas stream asynchronously and involved in complex heat exchange with it. Crystallization of particles is occurring under controlled rapid cooling conditions, ensures the formation of cellular-dendrite structures, local parameters of which are the subject of research in this article. Computer models for analysis of gas atomization process [1, 5-7] et al. exhibit almost complete agreement in describing the gas-dynamic and thermal parameters of the process and significantly differ in terms of the formation and growth of crystallites.

The nature of the redistribution of the alloying components between the phases is seen as the equilibrium one in a number of studies, i.e. occurring at full equalization of composition in liquid and solid phase, as opposed to nonequilibrium one, implemented under an additional condition of complete suppression of diffusion in the solid phase. In all cases, despite rapid crystallization conditions and deep supercooling of melt, it is using the local equilibrium conditions at phase interfaces.

Conditions of *local equilibrium* at the solid-liquid phase interface in the above-mentioned forced solidification modes get broken, when temperature, a composition of a liquid phase at the interface C_L* and composition of the crystallizing solid phase C_S* become dependent on the crystallization rate [3]. Values of phase diagrams parameters undergo the kinetically-dependent changes under *local nonequilibrium crystallization*, the nature of which depends on the relation of phase interface movement speed, diffusion rates of components in melt V_D and transfer of components across the phases interface V_{DI} [10-11].

In this paper, it is implemented a hybrid model, combining traditional analysis of heat transfer between molten particles and gas flow [8-9] with the thermodynamic and kinetic conditions at the front of the high-speed solidification [3, 10-11], which allows to identify the conditions of continuous transition from the local equilibrium diffusion-controlled dendrite structure to the local nonequilibrium diffusionless crystallization.

2. Formulation of a model

The models of microparticles solidification during gas atomization ([5-7] et al.) developed by several researchers are based on the description of equilibrium or local equilibrium crystallization of alloys.

The partition coefficient k_V in the local nonequilibrium model (subscript symbol *V*) [10-11] has the form:

$$k_V = \frac{k(1-\vartheta^2/V_D^2)+\vartheta/V_{DI}}{(1-\vartheta^2/V_D^2)+\vartheta/V_{DI}} \text{ at } \vartheta < V_D;\ k_V = 1 \text{ if } \vartheta \geq V_D. \quad (1)$$

Under conditions of local equilibrium, i.e. $\vartheta << V_D$ and $\vartheta << V_{DI}$, $k_V = k$ – equilibrium partition coefficient. An analogous relation is written for the slope of the liquidus line at local nonequilibrium model:

$$m_V = \frac{m}{1-k}\left(1-k_V+\ln\left(\frac{k_V}{k}\right)+(1-k_V)^2\frac{\vartheta}{V_D}\right) \text{ at } \vartheta < \mathrm{V_D}; \quad (2)$$

if $\vartheta \geq V_D$ then $m_V = m\dfrac{\ln(k)}{k-1}$. Under local equilibrium $m_V = m$, where m – equilibrium tangent of liquidus line angle.

Known values k_V (1) and m_V (2) allow to estimate corresponding change of non-equilibrium liquidus temperature for multicomponent alloys:

$$(T_L)_V = (T_L)_0 - \sum (m_V)_i\left[(C_L)_i - (C_0)_i\right], \quad (3)$$

as well as to reconstruct the geometry of nonequilibrium phase diagram, in particular, to determine the solidification range of a multi-component alloy Δt_{LS}:

$$(\Delta t_{LS})_V = \sum (m_V)_i (C_0)_i (1-(k_V)_i)/(k_V)_i \text{ at } \vartheta < V_D;$$
$$(\Delta t_{LS})_V = 0 \text{ at } \vartheta \geq V_D, \quad (4)$$

where $(T_L)_0$ – liquidus temperature of initial composition; $(C_0)_i$, $(C_L)_i$ – initial and current content of *i*-component in liquid phase.

The main components of the considered hybrid model are relations describing kinetics of formation of solid phase f_S and change in average composition of liquid phase, modified for conditions of local nonequilibrium crystallization of multicomponent alloys. The process of nucleation and growth of a new phase centers with specific density *N* describes by equation

$$\frac{df_S}{d\tau} = 4\pi(1-f_S)N\vartheta(\tau)R^2(\tau),$$

in which *R* – radius of growing crystallite and ϑ – growth rate is function of thermal supercooling melt $\Delta T(\tau)$. It's value is determined from the heat balance equation and used to estimate the speed of dendrite growth:

$$-V\rho(c\frac{dT}{d\tau} - L\frac{df_S}{d\tau}) = hS(T-T_g) + \sigma_0\varepsilon S(T^4 - T_g^4), \quad (5)$$

where *T*, T_g – absolute temperatures of melt and gas stream; *c*, *L* – volumetric heat capacity and heat of crystallization of the melt; τ – time of flight of the particle in the gas stream; *V*, *S* – volume and surface area of the particle; σ_0 – Stefan-Boltzmann constant; ε – emissivity factor of particle surface; *h* – convective heat transfer coefficient, estimated on the basis of gas-dynamic solving of task interaction of droplet with gas flow [8].

Linear crystallite growth rate determines the ratio $\vartheta = 2aP_T/R^*$[12], where *a* – thermal diffusivity of melt; P_T – thermal Peclet number; $P_T = Iv^{-1}(\frac{c}{L}\Delta T)$; $Iv(P) = Pexp(P)Ei(P)$ – Ivantsov relation of Peclet number *P*; R^*– radius of curvature of the top of the dendrite cell-crystallite in the accelerated crystallization, determined by the equation [12]:

$$R^* = \frac{\Gamma}{\sigma^*}\left[\frac{L}{c}P_T - \sum\frac{2(m_V)_i(C_0)_i(P_C)_i(1-(k_V)_i)}{1-(1-(k_V)_i)Iv(P_C)_i}\right]^{-1}, \quad (6)$$

where Γ – Gibbs-Thomson coefficient; σ^* – stability coefficient ($\sigma^* \approx 0.025$); $(P_C)_i = \vartheta R^*/2(D_L)_i$ – diffusion Peclet number; $(D_L)_i$ – diffusion coefficient of *i*-component in the melt; summation sign marks the additive contribution of the alloy components.

Redistribution of components between phases is calculated using equation, which correlates content of the melt at the phases interface C_L^* with kinetically dependent crystallization conditions [12]:

$$(C_L^*)_i = (C_0)_i/\left[1-(1-k_V)\mathrm{Iv}(P_C)_i\right]. \quad (7)$$

This makes it possible to evaluate the average composition of the residual liquid phase $(C_L)_i$ by using the equation, transformed for the conditions of rapid crystallization, subject to the availability of cross-border enriched layer of small thickness $\delta = 2D_L/\vartheta$, having a content $(C_L^*)_i$, different from $(C_L)_i$ [12]:

$$\frac{d(C_L)_i}{df_s} = \frac{(C_L)_i - (k_V)_i(C_L^*)_i}{1-f_s(1-\sigma_i(k_V)_i)};\ \sigma_i = \frac{2\alpha_i}{2\alpha_i+1};\ \alpha_i = \frac{8(D_S)_i\tau_{LS}}{\lambda_2^2}, \quad (8)$$

where $(D_S)_i$ – diffusion coefficient of *i*–component in the solid phase; τ_{LS} – local solidification time; λ_2 – the size of microcells (dendrite arm spacing). Introduction $0 \le \sigma_i \le 1$ parameter in equation (8) includes a partial diffusion in the solid phase of *i*-component.

During high-speed crystallization, when k_V value increases to one, the thickness of border enriched layer $\delta \approx 2D_L/\vartheta$ becomes comparable with magnitude of interatomic distances in crystal lattice of solid phase [3], the conditions for entrainment and complete "trapping" of the components at the interface formed and the limiting state $(C_L^*)_i=(C_S^*)_i=(C_0)_i$ achieved.

Formed model allows us to analyze the evolution of the solidification conditions and the redistribution of the components of the alloy crystallization, covering a wide range of cooling rates, within which a change of the alloy particle size is initiated and completed the transition from cellular-dendrite structure to flat front of diffusionless crystallization.

3. Experimental procedure

To investigate the crystallization conditions at gas atomization and type of thus formed structure it was selected martensitic stainless steel X12CrMoV. Physical-chemical and thermal characteristics of the alloy in the liquid and solid state were determined using the thermodynamic modeling software of phase transformations in multicomponent alloys «Polytherm» [12], as well as with published data. Table 1-2 shows parameters and thermal characteristics of the investigated alloy relating to the phase diagram.

Table 1. Parameters of equilibrium phase diagram of steel 12CrMoV.

Element	Partition coefficient	Tangent of liquidus line angle, K/mass. %
C	0.14	92.6
Mn	0.75	4.00
Si	0.76	22.9
Cr	0.89	1.45
Ni	0.86	5.13
Mo	0.67	3.10

Note: $N = 7.44 \cdot 10^{16}$ m^{-3}; $(D_S)_C = 3.9 \cdot 10^{-9}$ m^2/s; $(D_S)_{Si} = 4.1 \cdot 10^{-12}$ m^2/s (δ-Fe, 1400 °C).

Table 2. Thermal characteristics of the studied steel.

Parameter	Dimension	Value
Liquidus temperature	°C	1488
Solidus temperature	°C	1399
Thermal conductivity of the melt	W/(m·K)	27
Thermal conductivity in the solid state	W/(m·K)	37
Melt density	kg/m^3	6800
Density in the solid state	kg/m^3	7270
Specific heat capacity of the melt	J/(kg·K)	690
Specific heat of solid	J/(kg·K)	775
Specific latent heat of crystallization	KJ/kg	196.5

Crystallization parameters required for solving the task in the analysis of thermal processes, was given on the basis of estimates made in the work [13]: the specific density of nucleation N in the melt ranges $9 \cdot 10^{14}$–$3 \cdot 10^{17}$ m^{-3}, the rate constant of nuclei growth k_ϑ –

from $2 \cdot 10^{-2}$ to $6 \cdot 10^{-3}$ m/(K·s). The experimental values of secondary dendrite arm spacing for steel X12CrMoV [14] showed are depended from local value of the cooling rate by equation $\lambda_2 = 54.38 \vartheta_0^{-0,33}$.

Process conditions (initial melt temperature 1750 °C, the initial gas velocity of 1200 m/s, used gas - nitrogen) and the raw data to calculate the gas atomization process X12CrMoV alloy described in [8-9]; additionally specified V_D and V_{DI} values, which took characteristics: V_D = 17 m/s; V_{DI} = 3 m/s equal according estimations given in [10].

Investigations of the microstructure of the particles were carried out using an optical microscope Leica DMI5000 M at x50-x1000 magnifications, and scanning electron microscope (SEM) TESCAN Mira 3 LMU, operating at a magnification of x4 to $x10^6$ with accelerating voltage of from 200 V to 30 kV. SEM is equipped with Oxford Instruments for spectral energy-dispersive microanalysis (EDX) X-MAX^N based on nitrogen-free silicon drift X-ray detector.

To study dendrite structure of particles samples were pressed into an electrically conductive plastic, mechanically ground and polished, followed by etching with a solution containing 1.2 g NH_2SO_3H, 0.5-1 g NH_4FHF and 3 g of $K_2S_2O_5$, diluting with 100 ml of distilled water.

Research of local chemical heterogeneity and its quantitative analysis was carried out for particles with a diameter of 60 and 28.5 microns by constructing planar images distribution of elements with subsequent registration of content of test components in grid nodes, applied to an area the size 40x40 mm of particle area.

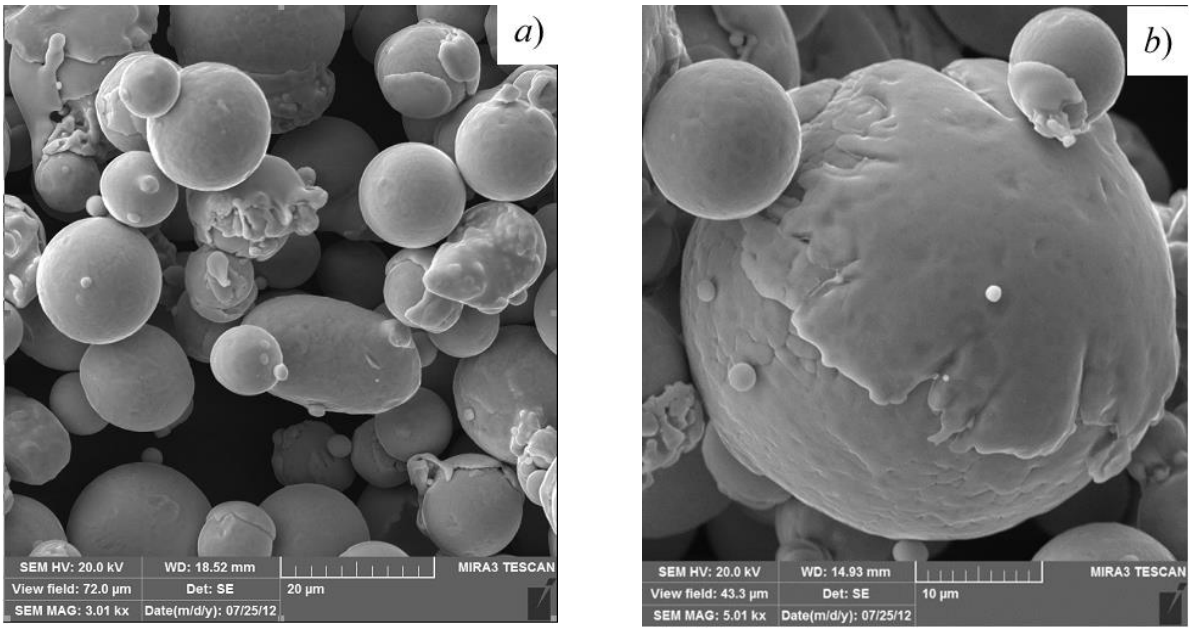

Figure 1. General view of X12CrMoV steel powder, received by gas atomization.

4. Characterization of atomized particles

General view of researched particles showed at Figure 1. Particles have near to spherical shape, some particles have satellites of smaller particles, which are attached to the surface of larger particles (Figure 1) or partially embedded therein (Figure 2,d) resulting in the collision (in solid state) and also during connection in liquid state (Figure 1,b).

Study of microsections at optical microscope showed that the particles have structure consisting of equiaxed dendrites (Figure 2,a-b) whose dimensions are on the periphery of the particle sizes do not differ from the central regions of dendrites. The collision of the particles, as shown by microsections (Figure 2,d), can initiate direction oriented cellular crystallites and their branching in the growth process.

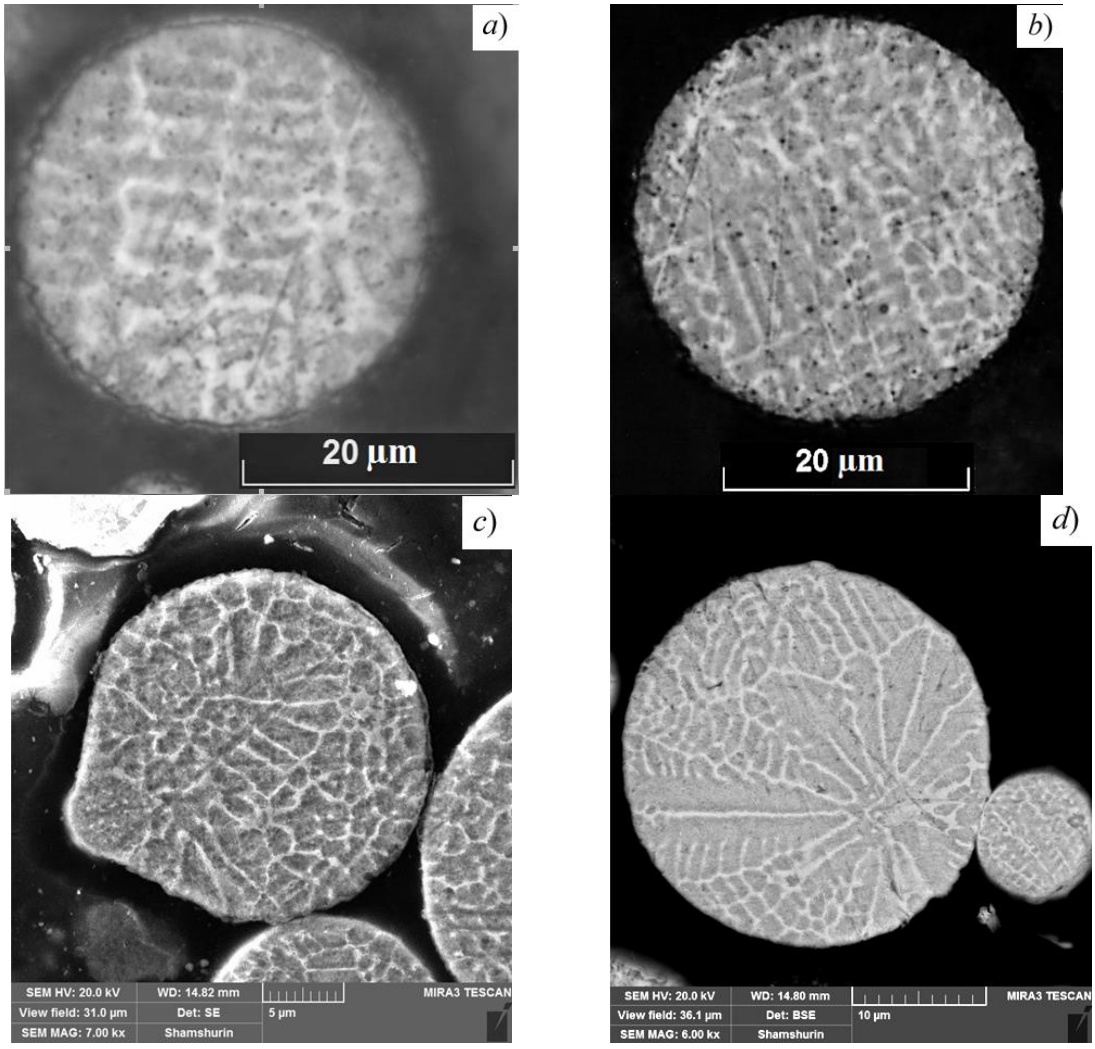

Figure 2. Cellular-dendrite microstructure of atomized powder Computer modelling results.

Computer analysis of thermal regime during solidification particles diameter of 10-100 microns alloys based on iron [8-9] shows that regular atomization modes provide substantial supercooling of the melt (50-120 K) and the cooling rate to 10^6-10^8 K/s.

Figure 3-4 shows the calculated solidification curves of steel X12CrMoV, which demonstrate the effect of most effective factors determining intensity of heat sink, supercooling of melt ΔT and average cooling rate during crystallization (Figure 4) at which the extrapolation gives for particle d = 1 mkm value V_0=10^8 K/s (Figure 4,c).

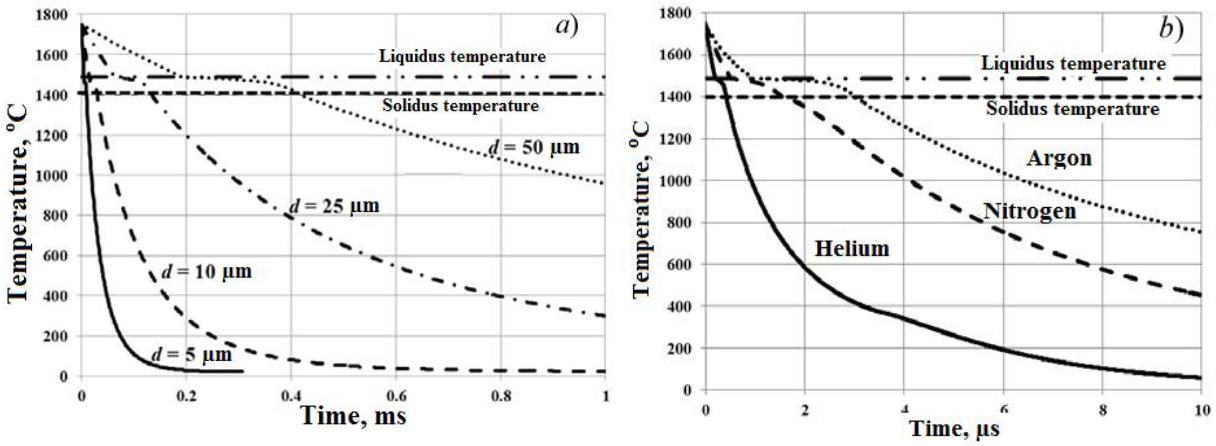

Figure 3. Thermal curves of solidification atomized particles depended of their size d (*a*) and (*b*) type of gas (for 50 mkm particle).

Summary results of the calculations (Table 3) show that decreasing particle size from 50 mkm to 1 mkm significantly increases the value of maximum supercooling ΔT_m and time of crystallization τ_{LS} is sharply reduced. This is due not only to the size of the particles, but also by increasing the heat transfer coefficient (from $1.2 \cdot 10^3$ to $800 \cdot 10^3$ W/m^2·K) due to the fact that small particles are solidified in a short period when their speed and therefore the heat transfer coefficient have the greatest value, whereas the larger particles begin to solidify later and crystallize at a significantly lower flow rate.

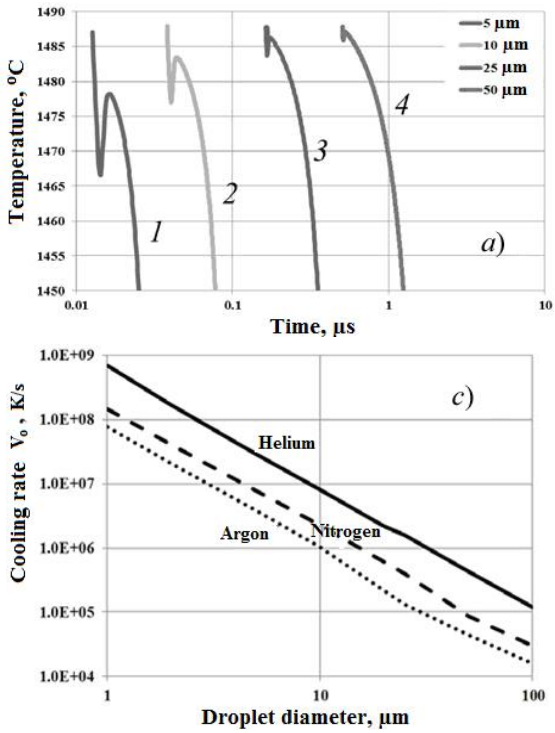

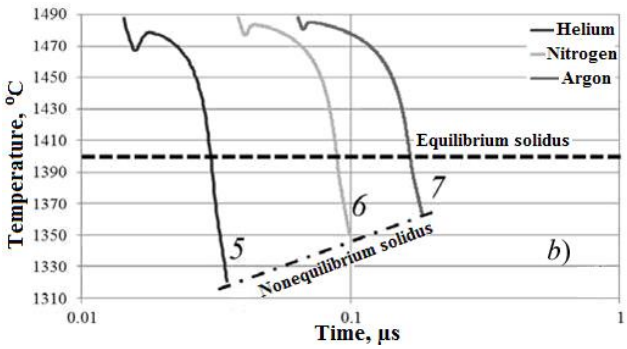

Figure 4. The dependence of initial supercooling ΔT (*a*-*b*) and average cooling rate V_0 (*c*) at solidification of particles different diameter (*a*, *c*) and different type of gas *d*, mkm: 5(*1*); 10(*2*); 25(*3*, *5* - *7*); 50(*4*) Gas: Helium (*5*); Nitrogen (*1*- *4*, *6*); Argon (*7*).

Deep supercooling during the crystallization of small particles (up to 100-120 K) causes an increase in the maximum cooling rate during the crystallization $(V_0)_m$, which varies from 10^5 (for d=50 mkm) to 10^9 K/s (for d<1.0 mkm). At the moment of maximum supercooling also maximum crystallization speed ϑ_m achieved, calculated value of that varies from $4 \cdot 10^{-4}$ (for d=50 mkm) to 10^2 m/s respectively. Reducing specific nucleation density (from $7.5 \cdot 10^{16}$ to $1.5 \cdot 10^{15}$ m^{-3}) causes to significant increasing of supercooling ΔT_m and growth rate ϑ_m.

Table 3. Parameters of crystallization and redistribution of carbon and silicon in according to the particle size.

Parameter	Particle diameter *d*, mkm				
	1.0	2.0	4.0	10.0	50.0
ΔT_m, K	100	83	68	52	27
τ_{LS}, mkm	1.67	5.13	15.5	67.4	1575
$(V_o)_m$, 10^6 K/s	176	54.2	16.8	3.52	0.13
ϑ_m, m/s	7.92	2.65	0.902	0.218	0.011
Carbon					
$(k_V)_C$	0.805	0.549	0.332	0.191	0.145
$(m_V)_C$, K/%	209	197	165	119	94.2
C_L*, % C	0.248	0.363	0.595	1.00	1.19
C_S*, % C	0.200	0.199	0.198	0.192	0.174
$(C_L)_m$, % C	0.205	0.224	0.269	0.365	0.635

Silicon					
$(k_V)_{Si}$	0.918	0.811	0.753	0.664	0.641
$(m_V)_{Si}$, K/%	28.4	27.4	25.6	23.8	22.9
C_L*, % Si	0.269	0.304	0.341	0.370	0.381
C_S*, % Si	0.247	0.247	0.247	0.246	0.244
$(C_L)_m$, % Si	0.266	0.277	0.283	0.284	0.287

Designations: ΔT_m – maximum supercooling; τ_{LS} – local time of crystallization; $(V_0)_m$ – the maximum average cooling rate at crystallization; ϑ_m – maximum linear rate of crystallization speed; $(C_L)_m$ – the maximum content of a component in residual liquid phase.

The maximum value of Biot number in all cases is much less than unity (Bi=0.004-0.02), indicating non-important temperature difference over cross section of particles and characterizes bulk crystallization conditions. This is consistent with observed in Figure 2,a-b unoriented cell-dendrite structure with uniform microcells sizes λ, which are traced experimentally by varying the particle diameter of 5 to 130 mkm (Figure 5).

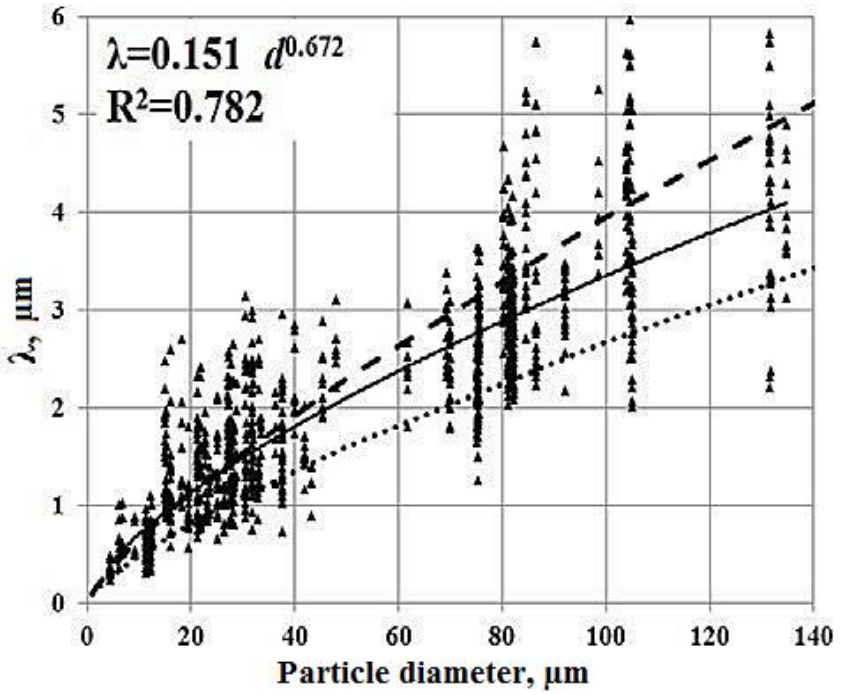

Figure 5. Dependence of dendrite secondary spaces λ_2 on particles diameter d in comparison with the calculation of [9] at initial gas velocity V_g = 100 (dotted line) and 1200 m/s (points). Line – statistical approximation of dependence λ(d) [9].

To identify boundary values of parameters that determine changes in conditions redistribution of components at the phases interface in Table 3 and Figure 6 a number of characteristics of the crystallization process is mapped depending on the diameter of particles on example carbon.

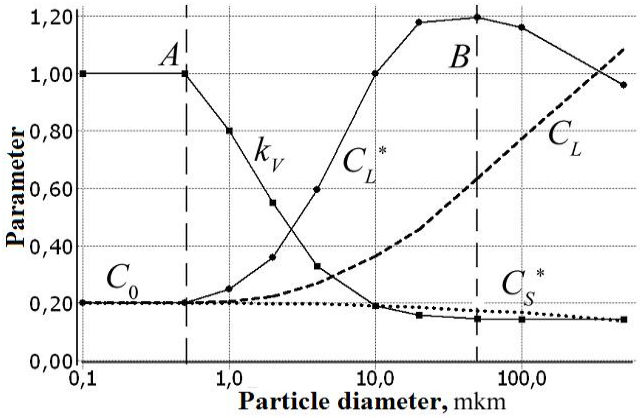

Figure 6. The effect of particle diameter d on the partition coefficient k_V, the carbon content C^*_L and C^*_S at the phases interface and the average composition of the liquid phase C_L (dotted line) during crystallization in nitrogen.

With increasing of particle diameter values of the partition coefficients are reduced from limit values $k_V = 1$ (at $d \leq A$) to equilibrium values (at $d \geq B$). In the same range of particle size (points A and B in Figure 6) there is an intensive change of liquid phase composition C^*_L at phases interface and solid phase composition C^*_S from the limits (C_L^*=C_S^*=C_0) at diffusionless crystallization (point A) to values that meet conditions of local equilibrium ahead of solidification front (point B).

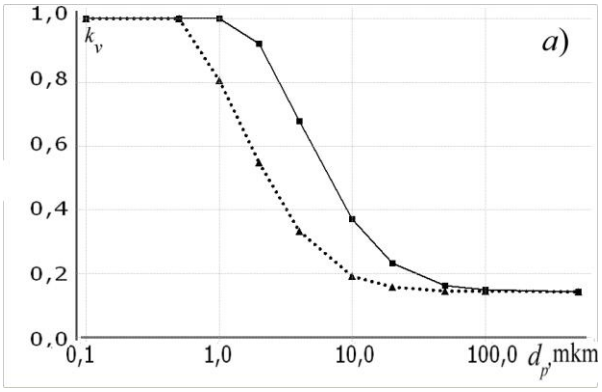

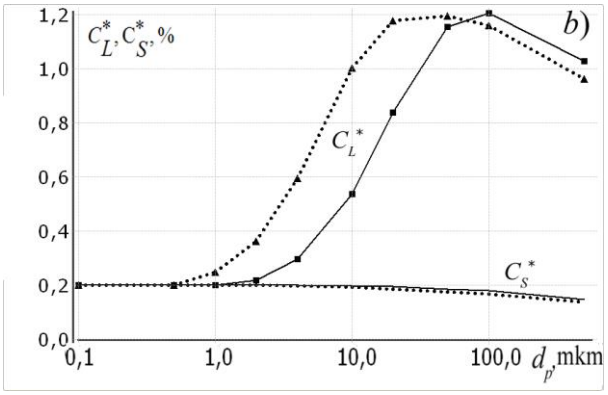

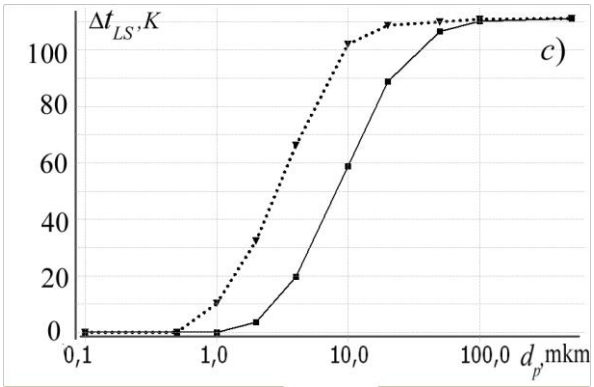

Figure 7. Dependency of distribution coefficient k_V (a), carbon concentration C_L^* and C_S^* in liquid and solid phase at the interface (b) and the solidification temperature interval $(\Delta t_{LS})_V$ (c) from particle diameter d_p and the type of working gas (line – He, dotted – Ar).

When used as a vehicle gas of argon and helium (Figure 6 - 7) a comparison of the curves k_V, C^*_L, C^*_S and $(\Delta t_{LS})_V$, depending on the diameter of the particles reveals a noticeable boundaries shift in the region of self-similarity mode at absolute stability (left to point A in Figure 6, where the change in diameter of particles has no effect at k_V =1, $(\Delta t_{LS})_V$ = 0,

$C_L^* = C_0$, $C_S^* = C_0$). A similar shift is occurring in the field of the dominant character of local equilibrium mode on the interface (right to point *B* with $k_V \approx k$, $\Delta t_{LS} \approx m C_0(1-k)/k$, $m_V \approx m$). This effect is due to the impact of more intensive heat sink, which is characteristic for helium with intensive heat transfer coefficient in the gas flow (see Figure 3,b and 4,b-c).

In order to assess microsegregation in solid phase it was made comparison of averaged data of silicon distribution across section of dendrite cells obtained by EDX, with the results of calculation (see Figure 8) [15], which takes into account diffusion suppression solid phase D_S in process of crystallization with local time τ_{LS} on the cross section of secondary dendrite space with size λ_2, whose value changes as a result of diffusion coalescence, described by the empirical equation $\lambda = K \tau_{LS}^n$ at $n = 0.33$.

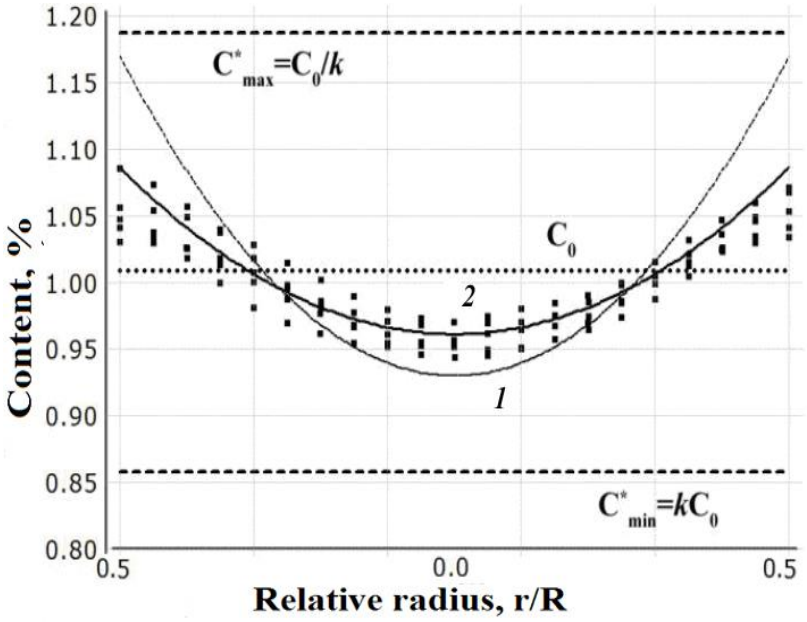

Figure 8. The silicon content distribution over the dendrite space cross section, according EDX (points) in comparison with simulation results (lines) at k = 0.76 (*1*) and k_V = 0.85 (*2*).

For atomized powder particles the agreement with the experimental data of the dendrite segregation of silicon is achieved (Figure 8) by using the partition coefficient k_V = 0.85–0.87 significantly exceeding the equilibrium value (k=0.76), which indicates the need to consider a significant contribution of nonequilibrium "trapping components" in the crystallization of particles diameter of 28-60 mkm, for which λ value is within 1.5-2.4 mkm and local time of crystallization from 0.55 to 1.85 mks, respectively.

5. Conclusion

As an important summary of the presented analysis, we can conclude that the studied thermal-physical conditions of gas atomization of melt (type and velocity of gas, supercooling of liquid, size of droplet and it's solidification rate et al.) not only indicate the influence on the formation of microstructure and chemical inhomogeneity of material but the ability to radical change the mode of components redistribution near the interface – from microsegregation to diffusionless type. This results indicate the ways and scopes for use of this technology in

order to implement the transient regimes of local nonequilibrium crystallization, providing the required level of structural and chemical homogeneity of atomized powder and articles made of them.

6. References

[1] Lavemia E and Srivatsan T 2010 The rapid solidification processing of materials: science, principles, technology, advances, and applications *J. Mater. Sci.* **45** 287-325
[2] Glezer A and Permyakova I 2012 *Nanocrystals, tempered from melt* (Moscow: Fizmatlit)
[3] Herlach D M, Galenko P and Holland-Moritz D 2007 *Metastable solids from undercooled melts* (Amsterdam: Elsevier)
[4] Laheniht F et al. 2010 Jet compaction - advanced steelmaking process for high quality alloys *Metallurgist* **10** 36-43
[5] Grant P S, Cantor B and Katgerman L 1993 Modelling of droplet dynamic and thermal histories during sprayforming Pt. 1 *Acta Metall. Mater.* **41** 3097-3108
[6] Hattel J H et al. 1999 A quasi-stationary numerical model of atomized metal droplets Pt. 1 *Mater. Sci. Eng.* **7** 413-430
[7] Vedovato G, Zambon A and Ramons E 2001 A simplified model for gas atomization *Mater. Sci. Eng. A* **304-306** 235-239
[8] Sufiiarov V Sh, Golod V M and Gjulihandanov E L 2012 Modelling of thermal and crystallization processes in the gas atomizatsin of iron-based alloys Proc. 9th Int. Conf. Foundry today and tomorrow 478-494
[9] Sufiiarov V Sh, Golod V M and Gjulihandanov E L 2013 Simulation the conditions of forming a dendritic structure iron-based alloys by gas atomization *Powder metallurgy and functional coatings* **2** 14-19
[10] Danilov D A and Galenko P K 2008 Diagram of morphological stability in the crystallization of a binary alloy *Bull. Udmurt University Physics. Chemistry* **1** 88-100
[11] Galenko P K et al. 2009 Dendritic solidification in undercooled Ni-Zr-Al melts: Experiments and modeling *Acta Mater.* **57** 6166-6175
[12] Golod V M, Savel'ev K D and Basin A S 2008 Modeling and computer analysis of crystallization of multicomponent iron-based alloys (Saint Petersburg: Polytechnic Univ Press)
[13] Pryds N H and Pedersen A S 2002 Rapid solidification of martensitic stainless steel atomized droplets *Metall. Mater. Trans.* **33** A 3755-61
[14] Volkova O, Heller H-P and Janke D 2003 Microstructure and cleanliness of rapidly solidified steels *ISIJ Int.* **43** 1724-1732
[15] Shin Y H et al. 2001 An analytical model of microsegregation in alloy solidification *ISIJ Int.* **41** 158-163